



HAL
open science

Investigation of the 3D crystalline network impact on the elastic properties of semi-crystalline polymers from a multi-scale modelling approach

E. Roguet, K. Akhan, N. Brusselle-Dupend, V. Le Corre, M. Sidhom, L. Cangémi, M. Moreaud, G. Clavier, V. Lachet, B. Rousseau

► To cite this version:

E. Roguet, K. Akhan, N. Brusselle-Dupend, V. Le Corre, M. Sidhom, et al.. Investigation of the 3D crystalline network impact on the elastic properties of semi-crystalline polymers from a multi-scale modelling approach. *Computational Materials Science*, 2019, 167, pp.77-84. 10.1016/j.commatsci.2019.05.006 . hal-02179256

HAL Id: hal-02179256

<https://ifp.hal.science/hal-02179256>

Submitted on 10 Jul 2019

HAL is a multi-disciplinary open access archive for the deposit and dissemination of scientific research documents, whether they are published or not. The documents may come from teaching and research institutions in France or abroad, or from public or private research centers.

L'archive ouverte pluridisciplinaire **HAL**, est destinée au dépôt et à la diffusion de documents scientifiques de niveau recherche, publiés ou non, émanant des établissements d'enseignement et de recherche français ou étrangers, des laboratoires publics ou privés.

Investigation of the 3D crystalline network impact on the elastic properties of semi-crystalline polymers from a multi-scale modelling approach

E. Roguet¹, K. Akhan¹, N. Brusselle-Dupend¹, V. Le Corre², M. Sidhom¹, L. Cangemi¹, M. Moreaud², G. Clavier^{1,3}, V. Lachet¹, B. Rousseau³

¹ IFP Energies nouvelles, 1 et 4 avenue de Bois-Préau, 92852 Reuil-Malmaison, France

² IFP Energies nouvelles, Rond-point de l'échangeur de Solaize, BP3, 69360 Solaize, France

³ Laboratoire de Chimie Physique, Université Paris-Sud, UMR 8000 CNRS, Orsay, France

Abstract

Nowadays, computational resources allow carrying out mechanical calculations on complex multi-scale materials. Finite Element (FE) calculations can especially be directly performed on microstructures of materials. This work is a first attempt to analyse the impact of the crystalline architecture at a mesoscopic scale on the macroscopic elastic properties of Semi-Crystalline Polymers (SCP). Such polymers can be considered biphasic materials, which are composed of an amorphous phase embedded in a crystalline network. The material studied here is Polyethylene (PE).

Molecular Dynamics (MD) calculations are carried out on a 100% crystallized Polyethylene model to determine the elastic properties of the crystalline regions of the material. 3D mesostructures of the typical layout of the spherulitic crystalline network of Semi-Crystalline Polymers are then constructed from experimental observations. These material data and this geometrical description are then integrated in computations with the Finite Element method on elementary volumes to finally determine the macroscopic elastic properties of the material. In this work, which is a first attempt to test such a multi-scale workflow, no amorphous phase is considered. Different 3D architectures are compared demonstrating the role of the crystalline arrangement on the stiffness of the material. Three main types of mesostructures have been analysed: crystalline lamellae disposed in a complete random arrangement, crystalline lamellae disposed in a spherulite arrangement, crystalline lamellae with branches disposed in a spherulite arrangement. It appears that the 3D configuration of the lamellae, as well as the presence of branches, have an influence on the macroscopic elastic properties of the material. Then, comparisons with experimental data suggest that the macroscopic elastic properties can be represented with a purely cohesive crystalline network for crystalline degree up to about 50%. This result questions the role of the amorphous phase on the elastic properties of such systems.

1. Introduction

This work addresses the general issue of the mechanical behaviour of Semi-Crystalline Polymers (SCP). These materials are widely used in engineering applications and the improvement of their mechanical properties is continuously researched due to the variety of application domains. To help for materials design, predicting the impact of the materials microstructure on their macroscopic mechanical properties is a challenge.

1 At the microscopic scale, various methods have been developed to investigate the structure of
2 SCP, for instance scanning electron microscopy or X-ray scattering [1-4]. Some studies have
3 been focused on understanding the involved crystallization mechanisms for a better
4 knowledge of their microstructural layout [5-7]. At the macroscopic scale, many works have
5 been done to model the mechanical response under several conditions such as pressure,
6 temperature or strain rate. Based on this description, many mechanical constitutive model
7 equations have been developed. Boyce et al. has proposed a model based on the polymer
8 chains kinetics for glassy polymers [9]. These authors introduce the decomposition of the
9 plastic flow into two kinds of resistances: an intermolecular resistance to stand for a segment
10 rotation and an entropic resistance to characterize the molecular alignment. Variations of the
11 original model have then been proposed to consider different experimental conditions [10-11]
12 and to modify the account of entanglements in the structure [12]. Microstructure
13 considerations have also been considered to model Semi-Crystalline Polymers (SCP)
14 behaviour. In literature, SCP are considered heterogeneous media with molecular chains that
15 can be part of a free amorphous phase, a crystalline network and/or an intermediate tied
16 amorphous phase [8]. Some approaches are based on a two phase representation of Semi-
17 Crystalline Polymers at the mesoscopic level which represent the material with a "solid"
18 network (including the crystal and the tied amorphous zone) interacting with a saturating
19 "soft" or fluid-like phase (essentially free amorphous) [13]. Micromechanical modelling based
20 on Eshelby theory [14] has also been developed within microstructures context. Applied to
21 polymer materials, this modelling allowed conclusive results on prediction of elastic
22 properties for Polypropylene (PP) or Polyethylene (PE) [15-16]. In this approach, the
23 crystalline lamellae are ellipsoidal inclusions whereas the amorphous phase is the matrix. The
24 same authors have also developed two-phase models where the inclusions are dispersed
25 randomly in the amorphous phase [16]. A three-phase model has also been developed by
26 Gueguen et al. [17] through a generalization of the double-inclusion model.
27
28
29
30
31

32 All these above mentioned works do not take into consideration the specific 3D architecture
33 of semi-crystalline materials at the mesoscopic scale, and in particular the presence of
34 spherulitic structures where lamellae grow radially from the nucleus of the spherulite in all
35 spatial directions, with some possible branches that grow from the principal lamellae. The
36 molecular origin of this branching and the consequent cross-hatched structure were clarified
37 by Lotz et al. [18] and such growth can be observed by optical microscopy or SEM.
38
39
40

41 Promising results obtained with previously described micromechanical models may suggest
42 that this particular structure of a semi-crystalline sample does not significantly affect the
43 macroscopic properties. However, other works suggest that the spherulites play an important
44 role in the deformation field [19-21]. For instance, Uchida et al. [22] proposed a Finite
45 Element homogenization method on multi-spherulitic structures; they concluded that the
46 distribution of lamellar orientation in the spherulite has an impact on the material behaviour.
47 Laschet et al. [23] have also proposed a two-level homogenization scheme to determine the
48 influence of the lamella design and of the crystalline properties on the effective properties of
49 spherulitic microstructures. An isotropic interface between spherulites has been introduced to
50 manage the spherulitic layout.
51
52
53

54 At first approximation SCP are two-phase materials, consisting of crystalline lamellae
55 embedded in amorphous phase. Only few papers tackle the role of the amorphous phase in the
56 mechanical macroscopic behaviour. The pioneering work of Struik [24-25], followed by
57 Chmelai et al. [4] evidences the heterogeneous nature of the amorphous phase, depending on
58 its confinement inside the rigid network of the crystal phase. This feature suggests
59
60
61
62
63
64
65

1 considering a free amorphous region with low mechanical properties and a confined one that
2 has a higher impact on the global rigidity. However, a recent work indicates that the
3 amorphous part does not have a major impact on the macroscopic elastic properties [26]. To
4 date, it is difficult to state the contribution of each phase on the overall elastic behaviour. The
5 aim of this paper is to analyse the qualitative role of the crystalline mesostructure, especially
6 the impact of the spherulite architecture on the macroscopic behaviour. Thus no amorphous
7 phase has been considered here. To achieve this objective, different mesostructures have been
8 designed from an in-house code and thanks to numerical calculations on them the
9 corresponding macroscopic elastic properties are determined and compared against each
10 other.
11

12
13 Method based on Finite Element (FE) or on Fast Fourier Transform (FFT) could be used to
14 carry out these calculations. This last approach has been originally introduced by Moulinec et
15 al. [27] and has been successfully used to compute numerically the properties of composite
16 materials [28-29]. However, in our work, the mesostructures are composed of lamella in
17 which the length, is significantly higher than the other dimensions. Besides, even if only the
18 crystalline phase is studied in this work, and contrary to the FE method, the FFT one imposes
19 to construct the all volume (even the void). It seems that, in our situation (slender structure in
20 a porous medium), the use of shell elements in a FE model is more suitable than a FFT
21 analysis.
22

23
24 To our knowledge, the originality of this work is the direct supply of input data obtained at
25 atomic scale from Molecular Dynamics (MD) simulation to the upper spherulitic scale, where
26 full field mechanical calculation results can give information about the role of the mesoscopic
27 architecture on the macroscopic properties. The method is based on a qualitative description
28 of the spherulitic structure and consists in a sensitivity analysis of the crystalline layout on the
29 macroscopic mechanical properties. Only the elastic properties are investigated in this first
30 work.
31
32

33
34 In the following, the inputs for the FE calculations are presented. The mesoscopic spherulitic
35 geometry of the models is deduced from observations of real microstructures from the
36 literature. The orthotropic elastic properties of the crystalline lamellae are determined
37 through MD simulations at the atomic scale. Then, the workflow employed to determine the
38 macroscopic properties is described and a Representative Volume Element (RVE) is
39 investigated in order to validate the size of the microstructure samples. Finally, macroscopic
40 elastic results are presented and compared for different crystalline arrangements. In order to
41 validate the proposed workflow with the FE method, some comparisons with a
42 micromechanical approach and with experimental results are also discussed.
43
44
45
46
47

48 **2. Input data for Finite Element calculations: mesostructures and** 49 **material properties**

50 **2.1 Mesostructures**

51
52 Semi-Crystalline Polymers, like PE, exhibit a hierarchical structure from nanoscopic to
53 microscopic scales as illustrated in Figure 1.
54
55
56
57
58
59
60
61
62
63
64
65

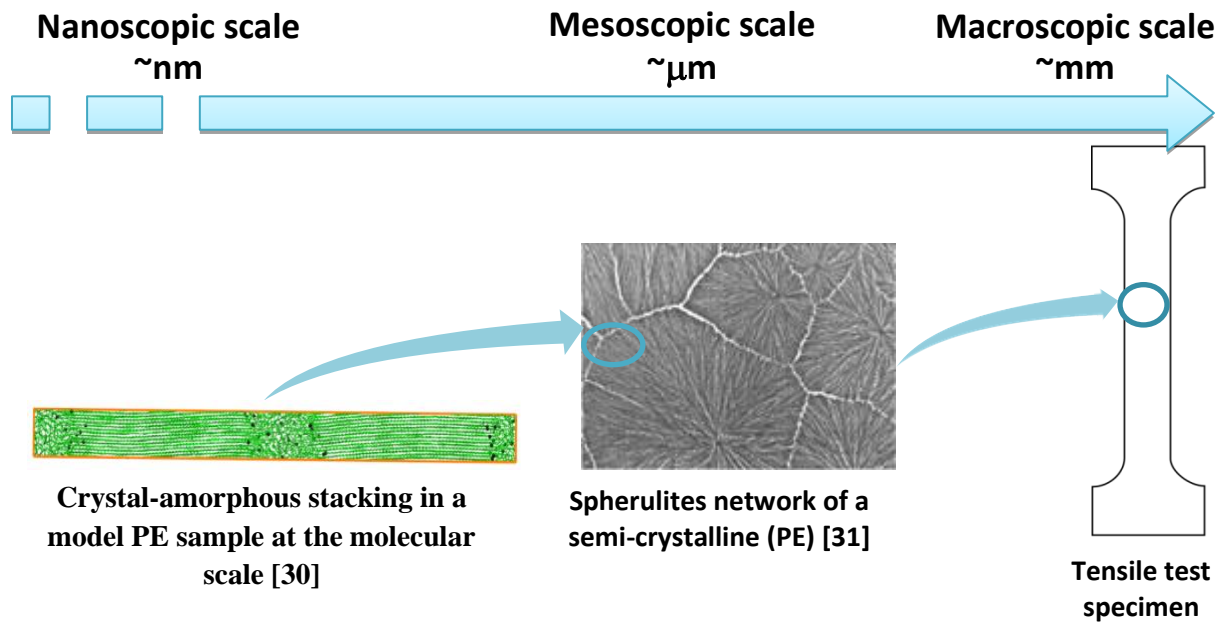


Figure 1: Schematic illustration of the structure of SCP at different length scales

At the nanometric scale, SCPs are considered in a first approximation as two-phase materials, consisting of crystalline lamellae embedded in amorphous phases. At the micrometric scale, an aggregation of spherulites, in which crystalline lamellae grow radially from the nucleus of the spherulite, can be observed. These mesoscopic structures are most often in contact with each other and represent a quite cohesive network. According to Atomic Force Microscopy (AFM) analyses, a cross-hatched structure can be observed within the spherulites (Figure 2). The spherulite sizes are dependent on the crystallization process. According to [32], lamellae are plate shape and following dimensions are considered to be reasonable values for PE: 1 μm length, 15 nm width and 5 nm thick.

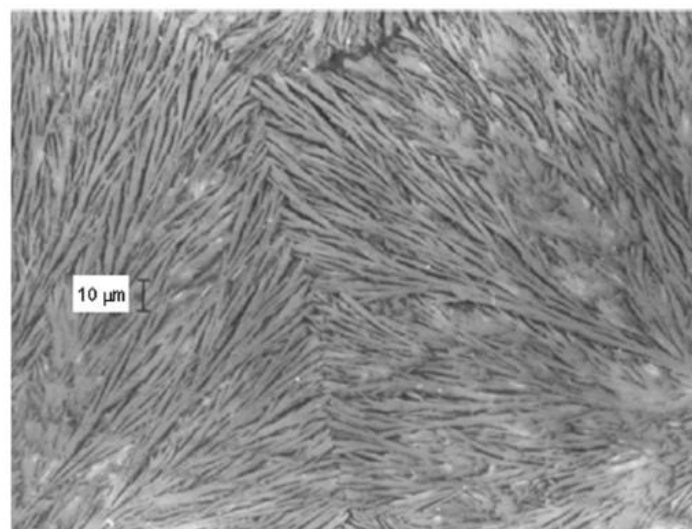


Figure 2: Cross-hatched structure of polypropylene's spherulites [33]

1 In this work, no amorphous phase is considered and only the crystalline network is
2 constructed and analysed. Different mesostructures are generated in order to understand and
3 analyse the impact of this meso-architecture on the material macroscopic behaviour.
4 Representative mesostructures are obtained thanks to mathematical morphology tools,
5 embedded in *plug Im!* software [34].
6

7 The impact of spherulite and cross-hatched arrangements is analysed. Three main types of
8 mesostructures are compared (Figure 3):
9

- 10 • “mesostructure type A” with a totally random distribution of lamellae
- 11 • “mesostructure type B” with a spherulite structure (only principal lamellae)
- 12 • “mesostructure type C” with a spherulite structure with branches (principal and
13 secondary lamellae resulting in a “cross-hatched” like structure)
14

15
16 To model mesostructures with a random lamellar network (Figure 3, type A), a Boolean
17 model with randomly oriented lamellae is considered first [35]. A Poisson Point process is
18 generated with a density imposed to follow the mesostructure overall degree of crystallinity.
19 At each point, a randomly oriented parallelepiped lamellae is implanted. This model needs
20 only five parameters :
21

- 22 - The generated volume size
- 23 - The size of the lamellae: length, width, thickness
- 24 - The degree of crystallinity
25

26
27 A second approach is used to model mesostructures with a lamellar spherulitic network
28 (Figure 3, types B). A Poisson Point process is first generated to model the germination
29 points. To complete the crystalline part generation, lamellae are then radially disposed, with
30 random orientation, from the cell’s centre defining germination point. The numbers of
31 germination points and of lamellae have to be adjusted to the desired degree of crystallinity.
32 This model needs several parameters to be adjusted :
33

- 34 - The generated volume size
- 35 - The number of germination points following degree of crystallinity
- 36 - The number of lamellae for each germination point, following also degree of
37 crystallinity
- 38 - The size of the lamellae: length, width, thickness
39

40
41 A third model is designed using the second one and by changing simple lamellae to lamellae
42 with branches (Figure 3, Type C). Additional parameters are the following :
43

- 44 - The number of branches for each principal lamella
- 45 - The geometry of the branches: length, width, thickness
- 46 - The branching angle: angle between the principal lamella and the secondary ones
47

48
49 A perfect load transfer between each connected entity has been considered. It is numerically
50 introduced by merging the connected lamellae with a perfect tie. The crystalline network is
51 cohesive through these connections despite the absence of the amorphous phase.
52

53
54 Illustrations of the three types of constructed mesostructures are proposed in Figure 3.
55
56
57
58
59
60
61

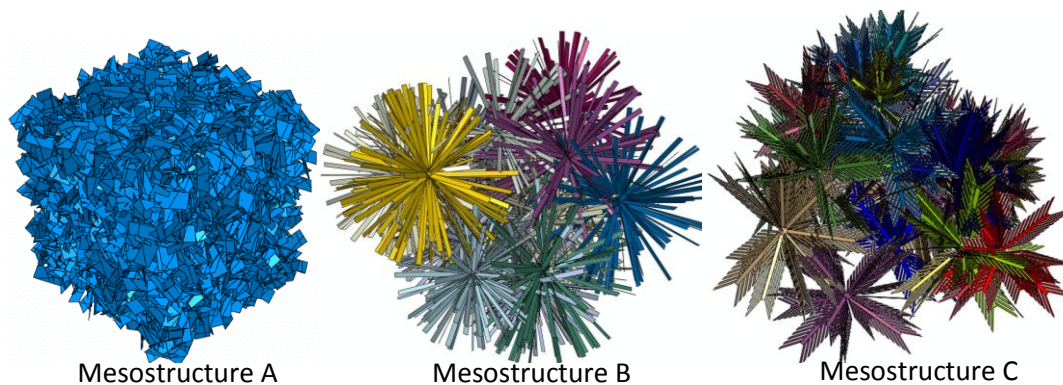


Figure 3: Three types of mesostructures

We define various quantities to characterize the mesostructures, and to allow comparisons between them. These indicators are: the degree of crystallinity (%), the size and number of lamellae, the number of germs and bifurcations in case of spherulitic structures, the specific surface area (nm^2/nm^3) and the features of the connection zones. The specific surface area is defined as the total surface of crystalline lamellae per volume unit of the mesostructure. The connection zones represent the regions where merging has been carried out to obtain a cohesive network. The number of connections/tied zones has been evaluated for each mesostructure. It defines the number of links between two entities of the structure, i.e. the number of links between two crystalline lamellae. Overlap zones can be either links between two lamellae belonging to two different spherulites or between two lamellae belonging to the same spherulite. This last type of connection cannot be found in the mesostructure B (see Figure 4). Note that the overlaps between a lamella of a spherulite and the corresponding germ are not considered in the count of connection zone, neither are the connections between a principal and a secondary lamellae in the case of mesostructure C.

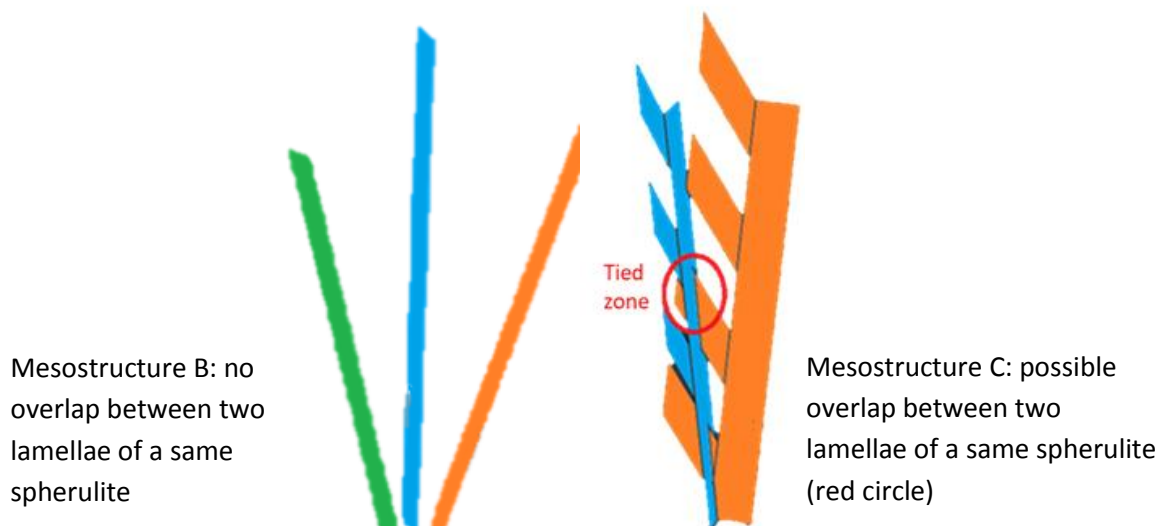


Figure 4: Connection zone inside a spherulite for mesostructures B and C, extracted from the geometry of figure 3.

2.2 Material inputs

The elastic properties of the PE crystalline phase have been determined at the atomic scale using MD calculations performed with the LAMMPS simulation package [36]. The PE crystal has been modelled using a simulation cell composed of 70 chains with 50 carbon atoms each

(= 5 x 7 x 25 PE unit cells). Periodic boundary conditions have been applied in the three space directions in order to mimic an infinite periodic crystal with infinite chain lengths. The Compass force field [37] has been used to account for bonded and non-bonded interactions. As discussed below, no Coulombic interactions have been considered.

A preliminary simulation has been conducted on a reference orthorhombic box in the isothermal-isobaric ensemble at 293 K and 1 bar in order to check the ability of the chosen force field to reproduce the lattice parameters of the PE crystal. Two calculations have been performed: one using the exact Compass force field including all partial charges and another one that neglects electrostatic contribution. Obtained parameters are respectively $a = 7.73 \text{ \AA}$, $b = 4.95 \text{ \AA}$, $c = 2.56 \text{ \AA}$ and $a = 7.72 \text{ \AA}$, $b = 4.96 \text{ \AA}$, $c = 2.57 \text{ \AA}$ for the two calculations. No significant impact of the partial charges is observed (error less than 0.5%). Obtained values in both cases are in good agreement with crystallographic data reported in reference [38] for PE at ambient conditions: $a = 7.417 \text{ \AA}$, $b = 4.945 \text{ \AA}$, $c = 2.547 \text{ \AA}$, with an overestimate of the lattice volume of ~5%. The Compass force field without electrostatic charges has thus been used thereafter for the study of the elastic properties of the crystalline PE.

The stiffness tensor elements (C_{ij}) of the crystalline PE have been calculated using an explicit deformation method that makes use of the generalised Hooke's law. Basically, different types of small elementary deformations (ϵ_j) are applied to the reference orthorhombic box, the stress tensor elements (σ_i) under each small deformation are then computed during a canonical simulation of 5 ns and the C_{ij} elements are extracted from the slope of the corresponding stress (σ_i) – strain (ϵ_j) plot. The following deformations were done:

- Three elementary uniaxial strains (one for each spatial direction) with 5 positive ϵ_j values, in the range (0 – 0.5) %, corresponding to a small extension of the material.
- Three elementary uniaxial strains (one for each spatial direction) with 5 negative ϵ_j values in the range (0 – 0.5) %, corresponding to a small compression of the material.
- Three elementary shearing strains (one for each box angle) with 5 positive ϵ_j values in the range (0 – 1) %.

More details about this procedure can be found in reference [39].

To illustrate these MD simulations, Figure 5 presents the stress–strain curves obtained in the case of the 10 uniaxial strain values performed in the direction of the crystallographic axis a. As required, a linear regime is observed in the range of deformations investigated in this work.

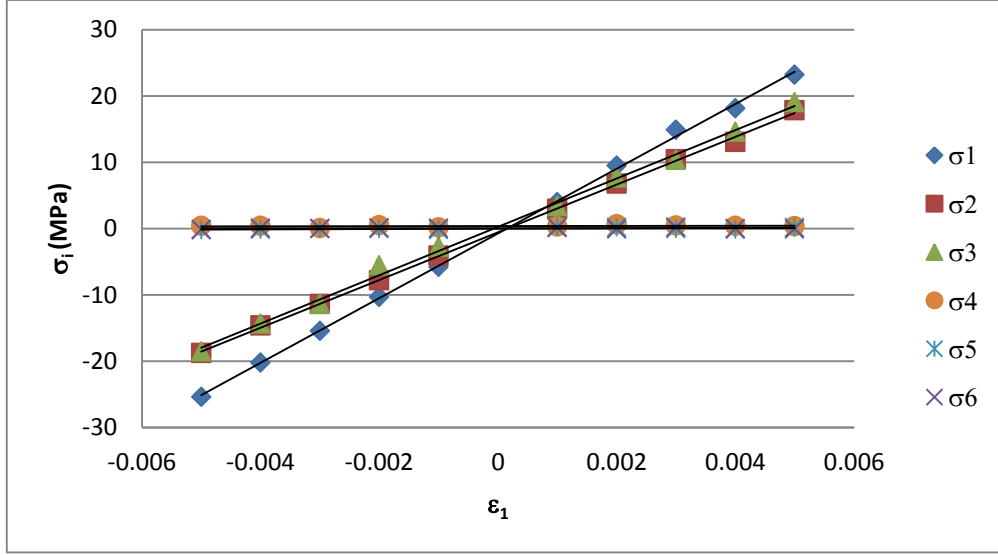


Figure 5: Stress–strain curves obtained from MD simulations of crystalline PE at 293 K in the case of an uniaxial strain ϵ_1 (direction of vector \mathbf{a} of the crystalline unit).

The obtained C_{ij} tensor, in Voigt notation, is:

$$\bar{\mathbf{C}} = \begin{bmatrix} 4.88 \pm 0.09 & 3.54 \pm 0.16 & 3.44 \pm 0.19 & 0.02 \pm 0.19 & 0.16 \pm 0.15 & -0.13 \pm 0.22 \\ 3.60 \pm 0.06 & 6.81 \pm 0.14 & 4.52 \pm 0.17 & -0.14 \pm 0.12 & -0.06 \pm 0.10 & -0.05 \pm 0.18 \\ 3.64 \pm 0.14 & 4.71 \pm 0.20 & 213.11 \pm 0.39 & 1.01 \pm 0.31 & 1.16 \pm 0.48 & -0.21 \pm 0.17 \\ 0.01 \pm 0.03 & -0.01 \pm 0.04 & -0.01 \pm 0.02 & 2.25 \pm 0.06 & 0.00 \pm 0.06 & 0.00 \pm 0.05 \\ 0.03 \pm 0.03 & 0.01 \pm 0.02 & -0.04 \pm 0.02 & 0.01 \pm 0.08 & 1.46 \pm 0.04 & 0.01 \pm 0.03 \\ 0.00 \pm 0.02 & 0.00 \pm 0.04 & 0.00 \pm 0.02 & 0.01 \pm 0.04 & 0.02 \pm 0.06 & 2.54 \pm 0.05 \end{bmatrix}$$

All values are expressed in GPa. Errors are confidence intervals on the slope of σ_i versus ϵ_i plot. The most important stiffness corresponds to the extension of the chains in the direction of their main axis, with $C_{33} = 213.11 \pm 0.39$ GPa. This result is quite close to experimental values founded in the literature (221 ± 8 GPa measured by x-ray diffractions [40]). Quite different results can be noted between the elements C_{34} and C_{43} or C_{35} and C_{53} . However, error bars associated with the C_{34} and C_{35} are large. With the exception of these two terms, we find that the lower-left and upper-right blocks of the tensor are zero within uncertainties. The same goes for the off-diagonal elements of the lower-right block. Orthotropic symmetry is thus assumed in the following and the corresponding nine C_{ij} coefficients are directly used in FE calculations to account for the elastic behaviour of the crystalline regions of the 3D mesostructures. Special attention has been paid to the orientation of the C_{ij} tensor in order to make the chain axis at the molecular level coincides with the chain axis at the mesoscopic level. At the mesoscopic level the chain axis is considered to be perpendicular to the surface of the crystalline lamellae (see Figure 6). Experimentally, the chains are found to be tilted by up to 45° from the lamellar normal, with 34° being the most common angle [41-42]. This tilt angle has not been considered in our simulations.

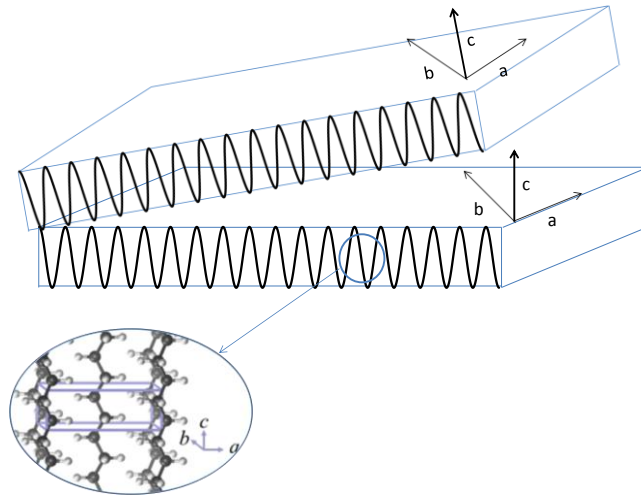


Figure 6: Schematic representation of the axis systems at the molecular and the mesoscopic scale with axis c being parallel to the chain axis i.e. perpendicular to the surface of the crystalline lamellae.

3. Workflow for FE calculations

Mesostructure architectures and material properties are the inputs for the FE calculations. The general workflow to carry out this up-scaling issue is proposed in the following scheme (Figure 7). The aim is to obtain elastic properties at the macroscopic scale and to determine the impact of the different mesostructures on these properties.

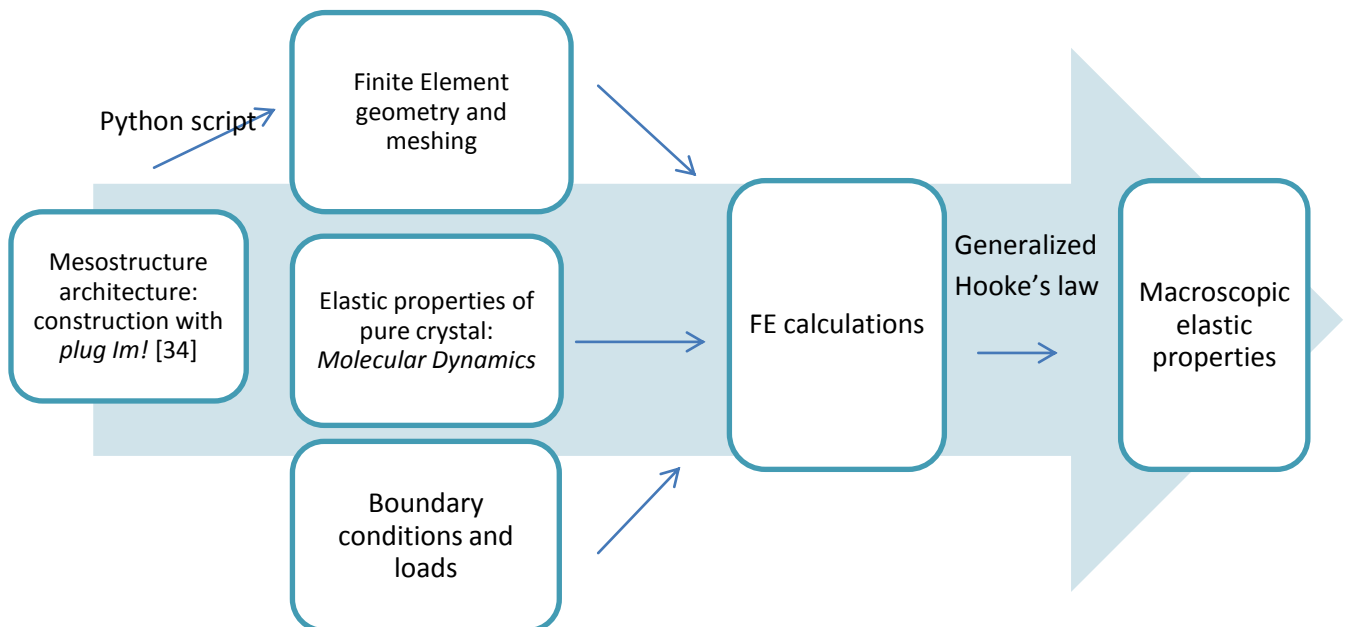


Figure 7: Schematic workflow of the study

3.1 Geometry and mesh generation

Once the mesostructure is created with *plug Im!*, the FE model is obtained by means of a python script. It allows defining the geometry (conform to *plug Im!*) and the mesh. Abaqus® Finite Element package is used to generate meshing and to perform simulations [43].

Three-node triangular general-purpose shell elements are used. The characteristic element size is chosen to have five elements in the lamella's width. With such a value, 300 000 elements were typically generated for a $400 \times 400 \times 400 \text{ nm}^3$ volume. It should be noted that the use of a FFT method would led to 64 million voxels (with also 5 pixels in the lamellae thickness, equivalent to 1 pixel by nm). Calculations have also been performed with three elements in the width to analyse the mesh size impact on mesostructure \mathbb{C} (it is assumed that if it is sufficient for the most intricate geometry, it is also the case for the others). The elastic properties (calculated as detailed in section 3.3) are proposed as supplementary data. Similar results are obtained for the two sizes of meshing. It seems reasonable to consider that the used mesh (typical size of five elements in the width) is accurate enough for this study.

3.2 Boundary conditions

This study aims at calculating the elastic properties of the mesostructures, i.e. at defining a relation between stress and strain tensors of the considered volume. By definition, the fourth-order elastic stiffness tensor \mathbb{C} is obtained by the following equation:

$$\frac{1}{V} \int_V \bar{\sigma} dV = \mathbb{C} : \frac{1}{V} \int_V \bar{\varepsilon} dV \quad \text{Equation 1}$$

The average values can be controlled by imposing values on the contour of the domain only, i.e. by imposing specific Boundary Conditions (BC).

Different kinds of BC have been evaluated for homogenization issues. Kinematic uniform boundary conditions (KUBC), obtained by constraining node displacements, tend to over-estimate the macroscopic stiffness. On the contrary, static uniform boundary conditions (SUBC) tend to under-estimate the stiffness. It is well known that periodic boundary conditions provide a better convergence than KUBC or SUBC [44]: the homogenized elastic properties will be obtained for a smaller RVE size with periodic boundary conditions. However, our mesostructures are not periodic and this type of BC cannot be applied easily. We thus decided to apply KUBC since it is known that, as far as the considered volume is important enough or the number of numerical simulations is important enough, the KUBC conditions converge towards the same result as the one obtained with periodic boundary conditions [44]. The KUBC conditions are applied through reference points: all the nodes of the same face are kinematically linked to a reference point. For an elongation along direction i , the displacement $u_i(x)$, with x being any node belonging to the face of normal direction i , is equal to the displacement u_i of the corresponding reference point.

At the macroscopic scale, the elastic behaviour is known to be isotropic. However, the local properties at the scale of a set of lamellae is necessarily anisotropic. A sufficient volume of material has to be considered in order to respect the global isotropic behaviour. To check if this assumption is verified, it has been decided to determine nine elastic properties (as an

orthotropic behaviour) and to check a posteriori if the three directions are equivalent. As an orthotropic behaviour is supposed, six elementary loadings determine the complete stiffness tensor:

- Three elementary uniaxial displacements (one for each spatial direction) with positive displacement in the range (0-10) nm.
- Three elementary shearing strains (one for each shear angle) with positive shear angle in the range (0-0.025) rad.

In each computation, the stress tensor elements are determined by the FE calculations and the C_{ijkl} elements are then extracted according to the generalized Hooke's law. Young moduli and Poisson's ratios are calculated from the uniaxial tests and shear moduli are determined from the shear test simulations.

3.3 Representative Volume Element: validity of the mesostructures

Ideally, the volume chosen for the mesostructures should be important enough to describe the statistics of the arrangement of the material leading to a so-called Representative Volume Element (RVE). In practice and due to calculation limitations, smaller volumes may be used and a statistical approach can be employed to converge towards the same results providing that a sufficient number of samples are considered.

The tested mesostructures are assumed to be ergodic and first of all, calculations are carried out to determine if the considered volumes are sufficient to lead to confident results. For each type of mesostructure (types A, B and C), several samples are constructed (with the same geometry parameters for a given mesostructure type) and for each sample, the macroscopic stiffness tensor is determined by means of six elementary loadings. The Voigt–Reuss–Hill averaging procedure [45] is then applied to provide average elastic constants (Young Modulus E_{VRH} , Shear Modulus G_{VRH} and Poisson's ratio ν_{VRH}). This averaging method combines the upper and lower bounds (respectively Voigt and Reuss averaging method : Young Modulus E_V/E_R , Shear Modulus G_V/G_R and Poisson's ratio ν_V/ν_R) by assuming that the average of the Voigt and the Reuss elastic constants is a good approximation for the macroscopic elastic constants :

$$E_{VRH} = \frac{E_V + E_R}{2} \quad G_{VRH} = \frac{G_V + G_R}{2} \quad \nu_{VRH} = \frac{E_{VRH}}{2G_{VRH}} - 1 \quad \text{Equation 2}$$

with

$$E_V = \frac{(A-B+3C)(A+2B)}{2A+3B+C} \quad G_V = \frac{(A-B+3C)}{5} \quad \nu_V = \frac{(A+4B-2C)}{4A+6B+2C} \quad \text{Equation 3}$$

$$E_R = \frac{5}{3A'+2B'+C'} \quad G_R = \frac{5}{4A'-4B'+3C'} \quad \nu_R = -\frac{2A'+8B'-C'}{6A'+4B'+2C'} \quad \text{Equation 4}$$

A, B, C, A', B' and C' depend on the fourth-order elasticity and compliance tensors (C_{ijkl} , S_{ijkl}) with the following equations in Voigt notation:

$$A = \frac{c_{11}+c_{22}+c_{33}}{3} \quad B = \frac{c_{12}+c_{13}+c_{23}}{3} \quad C = \frac{c_{44}+c_{55}+c_{66}}{3} \quad \text{Equation 5}$$

$$A' = \frac{s_{11}+s_{22}+s_{33}}{3} \quad B' = \frac{s_{12}+s_{13}+s_{23}}{3} \quad C' = \frac{s_{44}+s_{55}+s_{66}}{3} \quad \text{Equation 6}$$

The Reuss–Hill elastic properties are then calculated for each microstructure. In this RVE analyse, the main objective is to determine the confidence interval for the elastic properties. The relative error err_z for a property Z , depending on the volume V , can be estimated by the following equation [44]:

$$err_z = 2 * \frac{D_z(V)}{Z\sqrt{n}} \quad \text{Equation 7}$$

where n is the number of numerical samples, D_z is the variance of the property Z for a given volume V . The errors calculated for the elastic properties of each mesostructure configuration are given in Table 1.

	Mesostructure type A	Mesostructure type B	Mesostructure type C
Volume (nm ³)	500x500x500	400x400x400	400x400x400
Sample numbers	6	6	6
Statistical error on Young modulus (%)	5%	7%	7%
Statistical error on Poisson ratio (%)	10%	12%	12%
Statistical error on shear modulus (%)	3%	9%	5%

Table 1: Error estimations on macroscopic elastic properties for each mesostructure type

The different stiffness matrices are proposed as supplementary data. Undoubtedly, more samples or bigger volumes should be considered to have more precise values. However, the obtained estimations are considered to be sufficient to validate the workflow and to give insights for mesostructure-property relationships. Considering an uncertainty around 10%, the results are isotropic. According to this hypothesis, the elastic properties can be defined through only three parameters: Young moduli are given within 7%, Poisson’s ratio within 12% and shear modulus within 9% error.

4. Results

4.1 Mesostructure comparisons: impact of the 3D architecture

To understand the impact of the mesoscopic architecture, some structures of the three studied types are built with some identical features: a degree of crystallinity of 35%, a crystalline lamella width of 15 nm and a crystalline lamella thickness of 5 nm. All microstructural features of the different samples are gathered in Table 2. The volume of each mesostructure has been chosen to correspond to the values used in the previous section: 500x500x500 nm³ for mesostructure A and 400x400x400 nm³ for mesostructures B and C. The specific surface is approximately the same for the three architectures. Note that more lamellae are needed in mesostructure A to reach the same degree of crystallinity due to the bigger volume. The structural features of Table 2 are also given in terms of density: the tied zone density being the number of connection zones per volume unit. The structural quantity that allows distinguishing different structures seems to be the number of tied zones. There are very few tied zones in mesostructure A and this tendency is even accentuated when this value is normalized by the volume of the structure (500x500x500 nm³ for the mesostructure A

compared to $400 \times 400 \times 400 \text{ nm}^3$ for the others). The tied zones density in mesostructure A is about three times less than in mesostructure B and six times less than in mesostructure C.

Mesostructure type	A	B	C
<i>Microstructural features: plug Im! inputs</i>			
Degree of crystallinity (%)	35	35	35
Volume (μm^3)	0.125	0.064	0.064
Primary lamella number	6472	2841	1027
Secondary lamella number	/	/	8216
Germ number	/	24	9
<i>Microstructural features: plug Im! outputs</i>			
Specific surface ($\mu\text{m}^2/\mu\text{m}^3$)	72	72	69
Number of tied zones/connections	12915	19634	37077
Tied zones density (μm^{-3})	1.03E+05	3.07E+05	5.79E+05
<i>Macroscopic elastic properties</i>			
Average Young modulus (MPa)	56.6	98.7	142
Average Poisson's ratio	0.19	0.23	0.19
Average shear modulus (MPa)	23.8	45	64.3

Table 2: Features of the different studied mesostructures and corresponding elastic properties at room temperature and atmospheric pressure

Macroscopic elastic properties obtained following the workflow proposed in Figure 7 are also given in Table 2 for the different mesostructures (the complete stiffness matrices are provided as supplementary data). As mentioned above, an isotropic behaviour is observed within statistical uncertainty ($\sim 10\%$), thus, only average macroscopic Young modulus, Poisson's ratio and shear modulus are reported in Table 2. Despite this 10% uncertainty, tendencies can be discussed.

First, the crystallite distribution has an important influence on the material rigidity: the spherulitic mesostructure tends to strengthen the material (the Young Modulus of mesostructure B is 92% higher than the one of mesostructure A). At the same degree of crystallinity, a random disposition tends to be less rigid than a spherulitic one. This can be explained by the tied zone density: the random architecture is less cohesive and thus the elastic properties are weaker.

Then, comparing mesostructure C to mesostructure B, the impact of a cross-hatched like structure (approximated here with branches) can be analysed. Mesostructure C is more rigid than mesostructure B (the Young Modulus of mesostructure C is 44% higher than the one of mesostructure B). Once again, the number of tied zones density can explain such results as it is significantly higher in mesostructure C. It means that the connection links are more important when branches are taken into consideration and the cohesion of the material is improved. On the one hand, in the mesostructure B, there are only inter-spherulites connections: due to its construction (Figure 4), a lamella may only be connected to a lamella belonging to another spherulite. On the other hand, connection may be inter- and intra-spherulites in the mesostructure C. Due to the bifurcations in this mesostructure, tied zones can be either between lamellae belonging to two different spherulites or between two lamellae belonging to the same spherulite.

1 According to the obtained results, it appears that the architecture at the mesoscopic scale has
2 an influence on the elastic properties at the macroscopic scale. The spherulitic morphology
3 tends to strengthen the material and it seems that this stiffness increase may be linked to the
4 existing connections between spherulites (comparisons between mesostructures A and B).
5 Furthermore, the intra-spherulites connections have also an impact (comparisons between
6 mesostructures B and C). These two types of tied zones bring cohesion to the material and
7 thus influence its stiffness.
8

9 **4.2 Comparison with experimental data**

10 The numerical approach is not supposed to be predictive as the semi-crystalline polymer is
11 not completely modelled : only the crystalline phase is considered in this numerical analysis.
12 As a consequence, the direct comparison of numerical moduli with experimental results must
13 be analysed with care. The objective is to compare trends, order of magnitudes, and to give a
14 picture of the importance of the mesostructure on the elastic properties.
15
16

17 For a crystalline degree of 35%, available experimental data on PE provide a Young Modulus
18 of 83 (+/-6) MPa [32]. As a reminder, the results obtained with the proposed workflow are :

- 19 • 56 (+/-3) MPa for mesostructure A
- 20 • 99 (+/-7) MPa for mesostructure B
- 21 • 142 (+/-10) MPa for mesostructure C

22
23
24
25 All three mesostructures provide an elastic stiffness with a good order of magnitude. As only
26 crystalline network is here considered, this results question the amorphous phase role on the
27 elastic properties. This topic will also be discussed in the next section. Besides, one can
28 consider that mesostructure B provides the most predictive stiffness. At first sight, the
29 mesostructure C could have been considered as more realistic. However, mesostructure C
30 appears to be too stiff, but it can be argued that some geometric parameters may be modified.
31 Actually, whereas no geometrical parameter (as the lamellae size has been obtained through
32 Small-angle X-ray scattering [32]) may be modified in mesostructure B, some others may be
33 adjusted for mesostructure C: such as the size, the number and the orientation of the
34 secondary branches that have been arbitrarily chosen in this study. Experimental observations
35 like AFM analyses for instance [33] could be conducted on PE to have some experimental
36 inputs on secondary branches.
37
38
39
40

41 Elastic stiffness of additional structures of type B and C are assessed with different degrees of
42 crystallinity. The obtained mechanical properties are compared with experimental results [16,
43 32] and also to a micromechanical approach proposed by Bédoui [16] as shown in Figure 8.
44
45
46
47
48
49
50
51
52
53
54
55
56
57
58
59
60
61
62
63
64
65

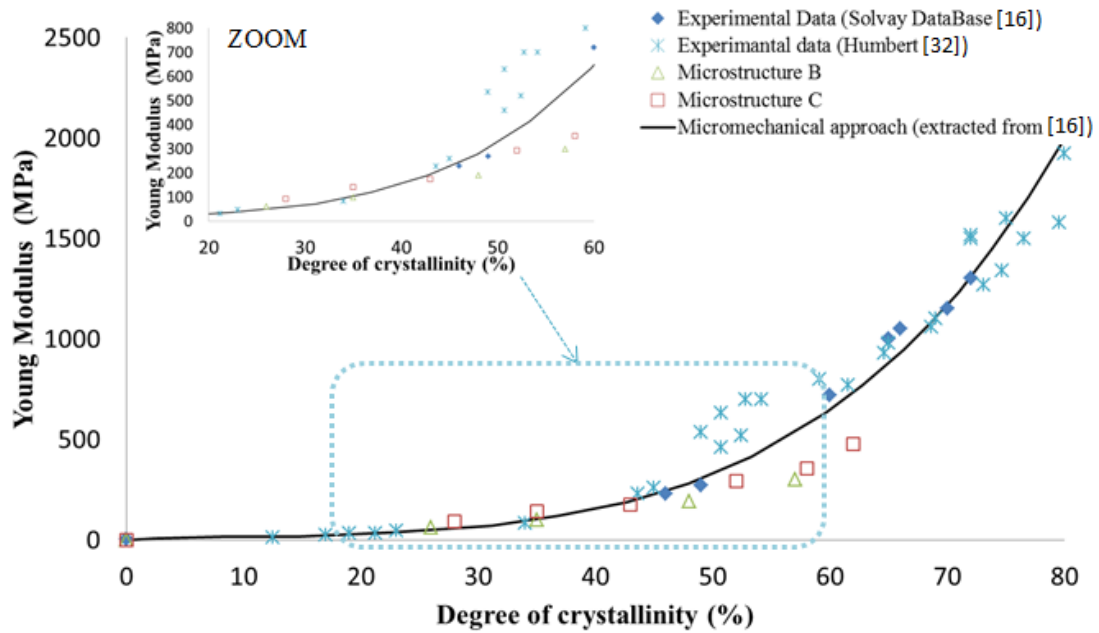


Figure 8: Comparison of experimental Young moduli from Solvay Database [16] and Humbert work [32] with numerical results and with a micro-mechanical model from Bédoui et al. [16]

Up to a degree of crystallinity of 50%, our results show good agreement with experimental results. Besides, the meso-architecture appears to have the same influence as previously described for the samples with a degree of crystallinity of 35% : the branching (mesostructure C) tends to strengthen the material (compared to architecture B) with an enhancement of the structural network both inside and outside the spherulites.

For higher degree of crystallinity, it is quite intricate to conclude: we did not manage to construct mesostructures with such amount of crystal due to numerical cost of the FE method. However, it seems reasonable to assume that our methodology will underestimate the Young modulus. It can be noticed that the inclusion-matrix model proposed by Bedoui et al. [16] allows interesting results: a very good estimation of the Young's modulus vs. crystallinity has been obtained (solid line in Figure 8). In this work, the authors considered the crystalline phase as a reinforcing phase embedded in an amorphous matrix. Crystal lamellae are approximated by ellipsoidal inclusions. To approximate the macroscopic tensor of the elastic behaviour of the equivalent homogeneous medium, the authors have used a differential scheme. In such approach, the reinforcing phase is introduced by infinitesimal increments using the dilute-distribution assumption [15]. Shape factors (width/thickness and length/thickness of lamellae) have been fitted to obtain very good agreement between model and experimental results. The chosen values (width/thickness=5 and length/thickness = 23) do not seem realistic compared to values observed in another work [32]. Besides, through this inclusion-matrix approach, the mesostructure architecture has no impact on the elastic properties, contrary to the results proposed in this work. However, what remains clear is that the Bédoui et al. model [16] provides better results and especially for high crystallinity rates.

Amorphous phase is not considered in the present work and the results seem better when the degree of crystallinity is low, which is surprising at first glance. Some works suggest that percolation in the crystalline network has an increasing role in the elastic macroscopic properties with increasing the degree of crystallinity, which counterbalances more and more

1 the role of the amorphous phase [26]. For degree of crystallinity higher than 50%, the
2 amorphous phase role should be less and less important as the crystallinity increases. Two
3 approaches may be explored to explain our results :

- 4 • The under-estimation of elastic properties at high degree of crystallinity can be
5 explained by the modification of geometric parameters: semi-crystalline polymers
6 with such a degree of crystallinity may have been obtained with larger lamellae
7 (which may be linked to a shape factor modification). The investigated
8 mesostructures may not be representative of the material with such a degree of
9 crystallinity and new sets of geometric parameters should be considered in future
10 works. Such an idea is supported by other works. Humbert et al. suggest that a
11 degree of crystallinity of 40% is a boundary for two different structural
12 morphologies : under 40%, spherulites contain both bundle-like and lamellar
13 crystals, above 40% spherulites are more well-defined [32].
- 14 • It can also be argued that amorphous phase can be in different state depending on the
15 crystalline network [4]. At low degree of crystallinity, the amorphous phase is
16 supposed to be less constrained and has a weaker behaviour which does not
17 influence sensibly the elastic properties. On the contrary, at higher degree of
18 crystallinity, the amorphous phase is more confined by the crystal lamellae: tied
19 amorphous phase is proportionally more important and may have more impact on
20 the elastic properties.
21
22
23
24
25
26
27
28

29 5. Conclusion

30 In this paper, a workflow has been proposed to determine elastic mechanical properties of
31 Semi-Crystalline Polymers. FE calculations have been carried out on representative
32 mesostructures. Some required inputs namely the elastic properties of the crystalline phase
33 have been calculated at the molecular scale thanks to MD simulations. According to the
34 results of the FE calculations, it is shown that the crystalline network geometry at the
35 mesoscopic scale has a major impact on the macroscopic mechanical behaviour. More
36 precisely, a spherulitic mesostructure tends to strengthen the material as the number of
37 cohesion points increases in comparison to a random architecture. The branching architecture
38 seems also to have an impact. Due to branches, connections between lamellae belonging to
39 the same spherulite is also possible: cohesion is given by inter and intra spherulite
40 interactions. Consequently, the branched structures have a higher Young modulus than
41 structures with no branches. Furthermore, in the studied cases and up to a degree of
42 crystallinity of 50%, the elastic properties of the crystalline network with no amorphous phase
43 show good agreement with macroscopic experimental properties. For higher degree of
44 crystallinity, the shift of the numerical values from the experimental data suggests that the
45 influence of the lamellae dimensions and/or of the percolation degree of the crystalline
46 network have to be deepened. The mechanical contribution of the constrained amorphous
47 phase should be investigated at this stage too. Additional numerical studies should be carried
48 out to analyse more precisely the role of the amorphous phase. A perfect load transfer has
49 here been considered between neighbouring spherulites, and the modification of this
50 behaviour may be tested to analyse the impact of this cohesion. Another way to consider the
51 amorphous phase should be the use of method with no need of discretization. For instance, a
52 method based on the Fast Fourier Transform can be tested.
53
54
55
56
57
58
59
60
61
62
63
64
65

In future work, the mesostructure construction could also be improved: it should be interesting to use experimental observation to create more realistic mesostructures. For example, the use of kinematic law to reproduce the spherulite growth could be introduced.

Supplementary data

The raw/processed data required to reproduce these findings cannot be shared at this time as the data also forms part of an ongoing study.

RVE size validation

Mesostructures A, B and C should not be compared: used material data are not the same, these results have only been used to check the RVE size.

Stiffness matrices (GPa) for several samples of mesostructure type A.

$$C_{ijkl} = \begin{bmatrix} 12.8 & 2.8 & 2.8 & 0 & 0 & 0 \\ 2.8 & 12.5 & 2.7 & 0 & 0 & 0 \\ 2.8 & 2.7 & 12.0 & 0 & 0 & 0 \\ 0 & 0 & 0 & 5.0 & 0 & 0 \\ 0 & 0 & 0 & 0 & 4.8 & 0 \\ 0 & 0 & 0 & 0 & 0 & 4.8 \end{bmatrix} \text{Mesostructure A-Draw 1}$$

$$C_{ijkl} = \begin{bmatrix} 12.4 & 2.7 & 2.7 & 0 & 0 & 0 \\ 2.7 & 11.9 & 2.6 & 0 & 0 & 0 \\ 2.7 & 2.6 & 11.1 & 0 & 0 & 0 \\ 0 & 0 & 0 & 4.9 & 0 & 0 \\ 0 & 0 & 0 & 0 & 4.6 & 0 \\ 0 & 0 & 0 & 0 & 0 & 4.6 \end{bmatrix} \text{Mesostructure A-Draw 2}$$

$$C_{ijkl} = \begin{bmatrix} 11.7 & 2.5 & 2.5 & 0 & 0 & 0 \\ 2.5 & 10.5 & 2.3 & 0 & 0 & 0 \\ 2.5 & 2.3 & 9.7 & 0 & 0 & 0 \\ 0 & 0 & 0 & 4.5 & 0 & 0 \\ 0 & 0 & 0 & 0 & 4.2 & 0 \\ 0 & 0 & 0 & 0 & 0 & 4.1 \end{bmatrix} \text{Mesostructure A-Draw 3}$$

$$C_{ijkl} = \begin{bmatrix} 10.9 & 2.4 & 2.4 & 0 & 0 & 0 \\ 2.4 & 10.6 & 2.3 & 0 & 0 & 0 \\ 2.4 & 2.3 & 9.9 & 0 & 0 & 0 \\ 0 & 0 & 0 & 4.5 & 0 & 0 \\ 0 & 0 & 0 & 0 & 4.1 & 0 \\ 0 & 0 & 0 & 0 & 0 & 4.0 \end{bmatrix} \text{Mesostructure A-Draw 4}$$

$$C_{ijkl} = \begin{bmatrix} 13.4 & 3.0 & 2.9 & 0 & 0 & 0 \\ 3.0 & 12.9 & 3.0 & 0 & 0 & 0 \\ 2.9 & 3.0 & 12.5 & 0 & 0 & 0 \\ 0 & 0 & 0 & 4.9 & 0 & 0 \\ 0 & 0 & 0 & 0 & 4.6 & 0 \\ 0 & 0 & 0 & 0 & 0 & 4.6 \end{bmatrix} \text{Mesostructure A-Draw 5}$$

$$C_{ijkl} = \begin{bmatrix} 13.3 & 3.0 & 2.9 & 0 & 0 & 0 \\ 3.0 & 13.2 & 2.9 & 0 & 0 & 0 \\ 2.9 & 2.9 & 11.6 & 0 & 0 & 0 \\ 0 & 0 & 0 & 5.3 & 0 & 0 \\ 0 & 0 & 0 & 0 & 4.8 & 0 \\ 0 & 0 & 0 & 0 & 0 & 4.9 \end{bmatrix} \text{Mesostructure A-Draw 6}$$

Stiffness matrices (GPa) for several samples of mesostructure type B.

$$C_{ijkl} = \begin{bmatrix} 0.11 & 0.03 & 0.03 & 0 & 0 & 0 \\ 0.03 & 0.10 & 0.03 & 0 & 0 & 0 \\ 0.03 & 0.03 & 0.12 & 0 & 0 & 0 \\ 0 & 0 & 0 & 0.04 & 0 & 0 \\ 0 & 0 & 0 & 0 & 0.05 & 0 \\ 0 & 0 & 0 & 0 & 0 & 0.05 \end{bmatrix} \text{Mesostructure B-Draw 1}$$

$$C_{ijkl} = \begin{bmatrix} 0.14 & 0.03 & 0.03 & 0 & 0 & 0 \\ 0.03 & 0.14 & 0.02 & 0 & 0 & 0 \\ 0.03 & 0.02 & 0.12 & 0 & 0 & 0 \\ 0 & 0 & 0 & 0.05 & 0 & 0 \\ 0 & 0 & 0 & 0 & 0.04 & 0 \\ 0 & 0 & 0 & 0 & 0 & 0.04 \end{bmatrix} \text{Mesostructure B-Draw 2}$$

$$C_{ijkl} = \begin{bmatrix} 0.13 & 0.03 & 0.03 & 0 & 0 & 0 \\ 0.03 & 0.14 & 0.03 & 0 & 0 & 0 \\ 0.03 & 0.03 & 0.13 & 0 & 0 & 0 \\ 0 & 0 & 0 & 0.06 & 0 & 0 \\ 0 & 0 & 0 & 0 & 0.06 & 0 \\ 0 & 0 & 0 & 0 & 0 & 0.05 \end{bmatrix} \text{Mesostructure B-Draw 3}$$

$$C_{ijkl} = \begin{bmatrix} 0.12 & 0.03 & 0.02 & 0 & 0 & 0 \\ 0.03 & 0.11 & 0.02 & 0 & 0 & 0 \\ 0.02 & 0.02 & 0.10 & 0 & 0 & 0 \\ 0 & 0 & 0 & 0.04 & 0 & 0 \\ 0 & 0 & 0 & 0 & 0.04 & 0 \\ 0 & 0 & 0 & 0 & 0 & 0.04 \end{bmatrix} \text{Mesostructure B-Draw 4}$$

$$C_{ijkl} = \begin{bmatrix} 0.14 & 0.01 & 0.01 & 0 & 0 & 0 \\ 0.01 & 0.10 & 0.03 & 0 & 0 & 0 \\ 0.01 & 0.03 & 0.10 & 0 & 0 & 0 \\ 0 & 0 & 0 & 0.05 & 0 & 0 \\ 0 & 0 & 0 & 0 & 0.04 & 0 \\ 0 & 0 & 0 & 0 & 0 & 0.05 \end{bmatrix} \text{Mesostructure B-Draw 5}$$

$$C_{ijkl} = \begin{bmatrix} 0.12 & 0.03 & 0.03 & 0 & 0 & 0 \\ 0.03 & 0.12 & 0.02 & 0 & 0 & 0 \\ 0.03 & 0.02 & 0.10 & 0 & 0 & 0 \\ 0 & 0 & 0 & 0.05 & 0 & 0 \\ 0 & 0 & 0 & 0 & 0.05 & 0 \\ 0 & 0 & 0 & 0 & 0 & 0.04 \end{bmatrix} \text{Mesostructure B-Draw 6}$$

Stiffness matrices (GPa) for several samples of mesostructure type C.

$$C_{ijkl} = \begin{bmatrix} 0.15 & 0.03 & 0.04 & 0 & 0 & 0 \\ 0.03 & 0.15 & 0.04 & 0 & 0 & 0 \\ 0.04 & 0.04 & 0.17 & 0 & 0 & 0 \\ 0 & 0 & 0 & 0.06 & 0 & 0 \\ 0 & 0 & 0 & 0 & 0.06 & 0 \\ 0 & 0 & 0 & 0 & 0 & 0.07 \end{bmatrix} \text{Mesostructure C-Draw 1}$$

$$C_{ijkl} = \begin{bmatrix} 0.18 & 0.05 & 0.04 & 0 & 0 & 0 \\ 0.05 & 0.17 & 0.04 & 0 & 0 & 0 \\ 0.04 & 0.04 & 0.14 & 0 & 0 & 0 \\ 0 & 0 & 0 & 0.08 & 0 & 0 \\ 0 & 0 & 0 & 0 & 0.06 & 0 \\ 0 & 0 & 0 & 0 & 0 & 0.05 \end{bmatrix} \text{Mesostructure C-Draw 2}$$

$$C_{ijkl} = \begin{bmatrix} 0.18 & 0.05 & 0.05 & 0 & 0 & 0 \\ 0.05 & 0.14 & 0.05 & 0 & 0 & 0 \\ 0.05 & 0.05 & 0.14 & 0 & 0 & 0 \\ 0 & 0 & 0 & 0.05 & 0 & 0 \\ 0 & 0 & 0 & 0 & 0.07 & 0 \\ 0 & 0 & 0 & 0 & 0 & 0.07 \end{bmatrix} \text{Mesostructure C-Draw 3}$$

$$C_{ijkl} = \begin{bmatrix} 0.13 & 0.03 & 0.03 & 0 & 0 & 0 \\ 0.03 & 0.15 & 0.03 & 0 & 0 & 0 \\ 0.03 & 0.03 & 0.14 & 0 & 0 & 0 \\ 0 & 0 & 0 & 0.05 & 0 & 0 \\ 0 & 0 & 0 & 0 & 0.07 & 0 \\ 0 & 0 & 0 & 0 & 0 & 0.07 \end{bmatrix} \text{Mesostructure C-Draw 4}$$

$$C_{ijkl} = \begin{bmatrix} 0.17 & 0.04 & 0.03 & 0 & 0 & 0 \\ 0.04 & 0.20 & 0.04 & 0 & 0 & 0 \\ 0.03 & 0.04 & 0.18 & 0 & 0 & 0 \\ 0 & 0 & 0 & 0.08 & 0 & 0 \\ 0 & 0 & 0 & 0 & 0.05 & 0 \\ 0 & 0 & 0 & 0 & 0 & 0.05 \end{bmatrix} \text{Mesostructure C-Draw 5}$$

$$C_{ijkl} = \begin{bmatrix} 0.15 & 0.03 & 0.04 & 0 & 0 & 0 \\ 0.03 & 0.15 & 0.04 & 0 & 0 & 0 \\ 0.04 & 0.04 & 0.17 & 0 & 0 & 0 \\ 0 & 0 & 0 & 0.06 & 0 & 0 \\ 0 & 0 & 0 & 0 & 0.06 & 0 \\ 0 & 0 & 0 & 0 & 0 & 0.07 \end{bmatrix} \text{Mesostructure C-Draw 6}$$

Mesh refinement

Stiffness matrices (GPa) for two identical samples with two different meshes

1
2 *Fine mesh :*
3

$$C_{ijkl} = \begin{bmatrix} 0.15 & 0.03 & 0.04 & 0 & 0 & 0 \\ 0.03 & 0.15 & 0.04 & 0 & 0 & 0 \\ 0.04 & 0.04 & 0.17 & 0 & 0 & 0 \\ 0 & 0 & 0 & 0.06 & 0 & 0 \\ 0 & 0 & 0 & 0 & 0.06 & 0 \\ 0 & 0 & 0 & 0 & 0 & 0.07 \end{bmatrix} \text{Mesostructure C-Finer mesh}$$

11
12
13 *Coarse mesh :*
14

$$C_{ijkl} = \begin{bmatrix} 0.16 & 0.04 & 0.04 & 0 & 0 & 0 \\ 0.04 & 0.16 & 0.05 & 0 & 0 & 0 \\ 0.04 & 0.05 & 0.18 & 0 & 0 & 0 \\ 0 & 0 & 0 & 0.07 & 0 & 0 \\ 0 & 0 & 0 & 0 & 0.06 & 0 \\ 0 & 0 & 0 & 0 & 0 & 0.07 \end{bmatrix} \text{Mesostructure C-Coarse mesh}$$

23
24 **Mesostructure comparisons**

25 *Stiffness matrices (GPa) for mesostructure A, B and C corresponding to the same material*
26 *data. Data used for the analyze of the mesostructure impact.*
27

28
29 *Mesostructure A*
30

$$C_{ijkl} = \begin{bmatrix} 0.06 & 0.01 & 0.01 & 0 & 0 & 0 \\ 0.01 & 0.06 & 0.01 & 0 & 0 & 0 \\ 0.01 & 0.01 & 0.06 & 0 & 0 & 0 \\ 0 & 0 & 0 & 0.03 & 0 & 0 \\ 0 & 0 & 0 & 0 & 0.03 & 0 \\ 0 & 0 & 0 & 0 & 0 & 0.02 \end{bmatrix} \text{Mesostructure A}$$

38
39
40 *Mesostructure B*
41

$$C_{ijkl} = \begin{bmatrix} 0.12 & 0.03 & 0.03 & 0 & 0 & 0 \\ 0.03 & 0.12 & 0.02 & 0 & 0 & 0 \\ 0.03 & 0.02 & 0.10 & 0 & 0 & 0 \\ 0 & 0 & 0 & 0.05 & 0 & 0 \\ 0 & 0 & 0 & 0 & 0.05 & 0 \\ 0 & 0 & 0 & 0 & 0 & 0.04 \end{bmatrix} \text{Mesostructure B}$$

50
51 *Mesostructure C*
52

$$C_{ijkl} = \begin{bmatrix} 0.15 & 0.03 & 0.04 & 0 & 0 & 0 \\ 0.03 & 0.15 & 0.04 & 0 & 0 & 0 \\ 0.04 & 0.04 & 0.17 & 0 & 0 & 0 \\ 0 & 0 & 0 & 0.06 & 0 & 0 \\ 0 & 0 & 0 & 0 & 0.06 & 0 \\ 0 & 0 & 0 & 0 & 0 & 0.07 \end{bmatrix} \text{Mesostructure C}$$

References

- [1] RH. Olley, D.C. Basset, An improved permanganic etchant for polyolefines, *Polymer* 23:1707 (1982).
- [2] L. Farge, J. Boisse, I. Bihannic, A. Diaz, S. Andre, Anisotropy development during HPDE necking studied at the microscale with in situ continuous 1D SAXS scans, *J. Polym. Sci. Part B: Polym. Phys.*, 56, (2018) 170-181. <https://doi.org/10.1002/polb.24527>
- [3] S. Humbert, O. Lame, J.M. Chenal, C. Rochas, G. Vigier. Small strain behavior of polyethylene: in situ SAXS measurements. *J. Polym. Sci. Part B: Polym. Phys.*, 48, (2010) 1535-1542. <https://doi.org/10.1002/polb.22024>
- [4] J. Chmelai, R. Pokorny, P. Schneider, K. Smolna, P. Belsky, J. Kosek, Free and constrained amorphous phases in polyethylene: Interpretation of ¹H NMR and SAXS data over a broad range of crystallinity, *Polymer*, 58: 189, (2015).
- [5] K. Yamada, S. Matsumoto, K. Tagashira, M. Hikosaka, Isotacticity dependence of spherulitic morphology of isotactic polypropylene, *Polymer* 39: 5327 (1998).
- [6] P.W. Zhu, G. Edward, Morphological distribution of injection-moulded isotactic polypropylene: a study of synchrotron small angle X-ray scattering, *Polymer* 45: 2603 (2004).
- [7] K. Nishida, T. Konishi, T. Kanaya, K. Kaji, Novel morphology of isotactic polypropylene crystal generated by a rapid temperature jump method, *Polymer* 45:1433 (2004).
- [8] P.J. Flory, D.Y. Yoon, and K.A. Dill. The interphase in lamellar semicrystalline polymers. *Macromolecules*, 17(4) (1984) 862–868.
- [9] M.C. Boyce, D.M. Parks, A.S. Argon. Large inelastic deformation of glassy polymers. Part I: rate dependent constitutive model, *Mechanics of Material*, 7 (1), (1998) 15-33.
- [10] M.C. Boyce, D.M. Parks, A.S. Argon. Plastic flow in oriented glassy polymers. *Int. J. Plast.*, 5 (6), (1989) 593-615.
- [11] Y. Tomita, S. Tanak. Prediction of deformation behavior of glassy polymers based on molecular chain network model. *Int. J. Solids Struct.*, 32 (23), (1995) 3423-3434.
- [12] E.M. Arruda, M.C. Boyce. A three-dimensional constitutive model for the large stretch behavior of rubber elastic materials, *J. Mech. Phys. Solids*, 41 (2), (1993) 389-412.
- [13] L. Cangémi, Y. Meimon. A Two-Phase Model for the Mechanical Behavior of Semicrystalline Polymers *Oil & Gas Science and Technology – Rev. IFP*, 56 (6), (2001) 555-580.

- 1
2
3
4
5
6
7
8
9
10
11
12
13
14
15
16
17
18
19
20
21
22
23
24
25
26
27
28
29
30
31
32
33
34
35
36
37
38
39
40
41
42
43
44
45
46
47
48
49
50
51
52
53
54
55
56
57
58
59
60
61
62
63
64
65
- [14] J.D. Eshelby. The determination of the elastic field of an ellipsoidal inclusion, and related problems, *Proc. Roy. Soc. Lond.* A241:376 (1957).
- [15] F. Bédoui, J. Diani, G. Régnier. Micromechanical modeling of elastic properties in polyolefins, *Polymer*, 45 (2004) 2433-2442.
- [16] F. Bédoui, J. Diani, G. Régnier, W. Seiler. Micromechanical modeling of isotropic elastic behavior of semicrystalline polymers, *Acta Materialia*, 54: (2006) 1513-1523.
- [17] O. Gueguen, S. Ahzi, A. Makradi, S. Belouettar. A new three-phase model to estimate the effective elastic properties of semi-crystalline polymers: application to PET. *Mech. Mater.* 42, (2010) 1–10.
- [18] B. Lotz, J.C. Wittmann, A.J. Lovinger. Structure and morphology of poly(propylenes): A molecular analysis. *Polymer*, 37, (1996) 4979-92.
- [19] C. G'Sell, J.M. Haudin. Introduction à la mécanique des polymères INPL, Nancy (1995).
- [20] J.Teixeira-Pinto, C. Nadot-Martin, F. Touchard, M.Gueguen, S. Castagnet. Towards the size estimation of a Representative Elementary Domain in semi-crystalline polymers, *Mechanics of Materials*, 95 (2016), 116-124.
doi.org/10.1016/j.mechmat.2016.01.003
- [21] H. Emre Oktay, E. Gürses. Modeling of spherulite microstructures in semicrystalline Polymers, *Mechanics of Materials*, 90, (2015), 83–101
doi.org/10.1016/j.mechmat.2015.04.010.
- [22] M. Uchida, T. Tsuruyo, N. Tada. Finite element simulation of deformation behavior of semi-crystalline polymers with multi-spherulitic mesostructure. *International Journal of Mechanical Sciences*, 52(2), (2010), 158-167.
- [23] G. Laschet, M. Spekowius, R. Spina, C. Hopmann. Multiscale simulation to predict microstructure dependent effective elastic properties of an injection molded polypropylene component, *Mechanics of Materials*, 105, (2017), 123–137.
- [24] Struik, L.C.E., 1987. The mechanical and physical ageing in semicrystalline polymers: 1. *Polymer*, 28, 1521-1533. [https://doi.org/10.1016/0032-3861\(87\)90353-3](https://doi.org/10.1016/0032-3861(87)90353-3)
- [25] Struik, L.C.E., 1987. The mechanical and physical ageing in semicrystalline polymers: 2. *Polymer*, 28, 1534-1542. [https://doi.org/10.1016/0032-3861\(87\)90354-5](https://doi.org/10.1016/0032-3861(87)90354-5)
- [26] B. Xiong, O. Lame, J.M. Chenal, C. Rochas, R. Seguela, G. Vigier, Amorphous phase modulus and micro-macro scale relationship in polyethylene via in situ SAXS and WAXS. *Macromolecules*, 48, (2015), 2149-2160.
<https://doi.org/10.1021/acs.macromol.5b00181>
- [27] H. Moulinec, P. Suquet. A fast numerical method for computing the linear and non linear mechanical properties of the composites. *Comptes rendus de l'Academie des Sciences, Serie II* 318(11), (1994) 1417–1423.

- 1
2
3
4
5
6
7
8
9
10
11
12
13
14
15
16
17
18
19
20
21
22
23
24
25
26
27
28
29
30
31
32
33
34
35
36
37
38
39
40
41
42
43
44
45
46
47
48
49
50
51
52
53
54
55
56
57
58
59
60
61
- [28] J. C. Michel, H. Moulinec, P. Suquet, A computational scheme for linear and non-linear composites with arbitrary phase contrast, *International Journal for Numerical Methods in Engineering* 52 (1–2), (2001), 139–158.
- [29] V. Vinogradov, G. W. Milton. An accelerated FFT algorithm for thermoelastic and non-linear composites, *International Journal for Numerical Methods in Engineering*, 76 (11), (2008) 1678–1695.
- [30] G. Clavier, Etude a l’échelle moleculaire des proprietes mecaniques de polymeres semi-cristallins. PhD Thesis in French, Université Paris-Saclay, (2017).
- [31] R.A. Pethrick. Morphology of crystalline polymers and methods for its investigation. *Polymer Structure Characterization: From Nano to Macro Organization*, The Royal Society of chemistry (2007) 107-140.
- [32] S. Humbert, O. Lame, R. Seguela, G. Vigier, A re-examination of the elastic modulus dependence on crystallinity in semi-crystalline polymers. *Polymer* 52:21 (2011), 4899-4909.
- [33] T. Voitot, Atomic Force Microscope study of plastic mechanisms in isotactic polypropylène beta. PhD Thesis in French, Université des Sciences et Technologies de Lille, 2000.
- [34] ”plug Im!” an open access and customizable software for signal and image processing. <https://www.plugin.fr>
- [35] H. Wang, A. Pietrasanta, D. Jeulin, F. Willot, M. Faessel, L. Sorbier, M. Moreaud. Modelling mesoporous alumina microstructure with 3D random models of platelets. *Journal of Microscopy*, Wiley, 260 (3), (2015), 287-301. <https://doi.org/10.1111/jmi.12295>
- [36] S.J. Plimpton, Fast Parallel Algorithms for Short-Range Molecular Dynamics, *J. Comp. Phys.*, 117, (1995), 1-19. <http://lammps.sandia.gov>.
- [37] H. Sun, COMPASS: An ab Initio Force-Field Optimized for Condensed-Phase Applications - Overview with Details on Alkane and Benzene Compounds, *J. Phys. Chem. B*, 102, (1998), 7338-7364.
- [38] A.J. Peacock, *Handbook of Polyethylene: Structures: Properties, and Applications*, Marcel Dekker Inc., New-York (2000).
- [39] G. Clavier, N. Desbiens, E. Bourasseau, V. Lachet, N. Brusselle-Dupend, B. Rousseau. Computation of elastic constants of solids using molecular simulation: comparison of constant volume and constant pressure ensemble methods, *Mol. Sim.*, 43, (2017), 1413–1422.
- [40] M. Matsuo, C. Sawatari. Elastic modulus of polyethylene in the crystal chain direction as measured by X-ray diffraction. *Macromolecules*, 19 (7), (1986), 2036-2040.
- [41] J.-J. Point, J. Rault, J.D. Hoffman, A.J. Kovacs, L. Mandelkern, B. Wunderlich, et al. General discussion. *Faraday Discussions of the Chemical Society* 68, (1979), 365-490.

- 1
2
3
4
5
6
7
8
9
10
11
12
13
14
15
16
17
18
19
20
21
22
23
24
25
26
27
28
29
30
31
32
33
34
35
36
37
38
39
40
41
42
43
44
45
46
47
48
49
50
51
52
53
54
55
56
57
58
59
60
61
62
63
64
65
- [42] E. F. Oleinik, Plasticity of Semicrystalline Flexible-Chain Polymers at the Microscopic and Mesoscopic Levels, *Polymer Science Series C*, 45, (2003), 17-117.
- [43] Abaqus Unified FEA <https://www.3ds.com/products-services/simulia/products/abaqus/>
- [44] T. Kanit, S. Forest, I. Gallier, V. Mounoury, D. Jeulin. Determination of the size of the representative volume element for random composites: statistical and numerical approach. *IJSS* 40, (2003), 3647-3679.
- [45] J.M.J. den Toonder, J.A.W. van Dommelen and F.P.T. Baaijens. The relation between single crystal elasticity and the effective elastic behaviour of polycrystalline materials: theory, measurement and computation. *Modelling Simul. Mater. Sci. Eng.* 7 (1999), 909–928.